One dimensional dynamics of the d electrons in alpha-NaV2O5

Atzkern, S.; Knupfer, M.; Golden, M.S.; Fink, J.; Yaresko, A.N.; Antonov, V.N.; Hübsch, A.; Waidacher, C.; Becker, K.W.; von der Linden, W.; Obermeier, G.; Horn, S.

Published in:
Physical Review B

One-dimensional dynamics of the *d* electrons in α'-NaV_2O_5

S. Atzkern, M. Knupfer, M. S. Golden, and J. Fink
Institute for Solid State Research, IFW Dresden, P.O. Box 270016, D-01171 Dresden, Germany

A. N. Yaresko* and V. N. Antonov*
Max-Planck-Institut für Physik komplexer Systeme, Nöthnitzer Str. 38, D-01187 Dresden, Germany

A. Hübsch, C. Waidacher, and K. W. Becker
Institut für Theoretische Physik, Technische Universität Dresden, D-01062 Dresden, Germany

W. von der Linden
Institut für Theoretische Physik, Technische Universität Graz, Petersgasse 16, A-8010 Graz, Austria

G. Obermeier and S. Horn
Institut für Physik, Universität Augsburg, D-86159 Augsburg, Germany
(Received 8 November 2000; published 5 April 2001)

We have studied the electronic properties of the ladder compound α'-NaV_2O_5, adopting a joint experimental and theoretical approach. The momentum-dependent loss function was measured using electron energy-loss spectroscopy in transmission. The optical conductivity derived from the loss function by a Kramers-Kronig analysis agrees well with our results from local spin density approximation (LSDA) $+U$ band-structure calculations upon application of an antiferromagnetic alignment of the V $3d_{xy}$ spins along the legs and an on-site Coulomb interaction U between 2 and 3 eV. The decomposition of the calculated optical conductivity into contributions from transitions between selected energy regions of the density of states reveals the origin of the observed anisotropy of the optical conductivity. In addition, we have investigated the plasmon excitations related to transitions between the vanadium states within an effective 16-site vanadium cluster model. Good agreement between the theoretical and experimental loss functions was obtained using the hopping parameters derived from the tight-binding fit to the band-structure and moderate Coulomb interactions between the electrons within the *ab* plane.

DOI: 10.1103/PhysRevB.63.165113 PACS number(s): 71.10.Fd, 71.20.−b, 71.27.+a, 71.45.Gm

I. INTRODUCTION

In 1996 M. Isobe and Y. Ueda[1] published magnetic-susceptibility measurements of α'-NaV_2O_5 powder samples, proposing the existence of linear antiferromagnetic spin-1/2 chains and a possible spin-Peierls transition at a critical temperature, $T_c = 34$ K. The original picture of the charge ordering in this mixed valence ladder compound was that of alternating legs of V^{4+} and V^{5+} ions.[2] However, a recent determination of the crystal structure using single-crystal x-ray diffraction at room temperature[3,4] yielded only one symmetrically inequivalent vanadium ($V^{4.5+}$) position. Due to the observed one-dimensional character of the spin and charge system at room temperature—which was by that time also confirmed by inelastic neutron-scattering[5,6] and angle-resolved photoemission experiments[7]—the picture of linear chains of V-O-V rungs containing a single *d* electron in a molecular orbital-like state with antiferromagnetic alignment along the ladders has increasingly won recognition. Below T_c charge ordering has been observed in ^{51}V NMR studies,[8] but the ordering pattern has not yet been defined. Calculations of the electronic ground state[9,10] have predicted a zigzag charge ordering along the ladders and only lately, with the support of the most recent experimental data[11–14] does the evidence for zigzag order appear to outweigh that for more complicated order patterns.[15] Nevertheless, there remain a number of important, open questions such as the nature of the correlations between the charges and spins which are the driving force for the observed charge ordering and which make the system insulating.

The electronic structure of α'-NaV_2O_5 has been intensively studied experimentally by means of optical absorption[16] and reflectivity,[17,18] as well as theoretically within the framework of band-structure calculations[3,19–21] and exact diagonalization techniques.[22–24] Nevertheless, there is a controversial discussion about the origin of the electronic excitations in this system. For example, concerning the absorption peak occurring at about 1 eV in optics, transitions between bonding and antibonding combinations of V $3d_{xy}$ states,[3,17,25] transitions between vanadium states of different symmetry,[18] as well as on-site *d*-*d* transitions between crystal-field-split vanadium $3d$ states,[16] have been proposed as the origin of this feature. Furthermore, the information from the experiments still appears to be insufficient to enable the definition of a unique parameter set for the description of the electronic structure of α'-NaV_2O_5. In particular, independent of which theoretical model was used, significantly different values for the on-site Coulomb repulsion U, the intersite Coulomb repulsion V_{xy} between electrons on legs of adjacent ladders and the hopping parameter t_{xy} have been discussed in the literature (for a comparison see Table I). Since the charge ordering as well as the charge transport properties strongly depend on the energies described by these parameters, a more exact determination of their values could lead to a better understanding of the elec-

TABLE I. Literature values for the hopping parameters t, the on-site Coulomb interaction U, and the intersite Coulomb interactions V_α compared with the results of this work.

Ref.	t_a	t_b	t_{xy}	U	V_a	V_b	V_{xy}
Smolinski *et al.*, Ref. 3	0.38	0.17	0.012	2.8			
Horsch *et al.*, Ref. 25	0.35	0.15	0.3	4.0			
Damascelli *et al.*, Ref. 17	0.3	0.2					
Nishimoto *et al.*, Ref. 23	0.3	0.14	0.05	4.0		0.5	
Popovic *et al.* Ref. 19				6.82			
Cuoco *et al.* Ref. 22	0.4	0.2	0.15	4.0	0.8	0.8	0.9
Sa *et al.* Ref. 50	0.38	0.17	0.012	2.8	0.37	0.10	0.43
This work	0.38	0.17	0.012	2.8	0.8	0.6	0.9

tronic properties of α'-NaV_2O_5.

In this contribution, we present a joint experimental and theoretical investigation of the electronic excitations and their momentum dependence in α'-NaV_2O_5 , measured using high-resolution electron energy-loss spectroscopy in transmission. The comparison of the data with models based both on the local spin density approximation (LSDA) $+U$ formalism, as well as a cluster approach, enable the construction of a consistent theoretical description of the electronic structure of α'-NaV_2O_5, and result in the determination of a double-checked parameter set. The paper is organized as follows. In Sec. II the experimental and theoretical methods are introduced. Section III contains the presentation and discussion of the experimental and theoretical results and is split into subsections dealing with the different aspects of the data. Last, Sec. IV is a summary.

II. METHODOLOGY

A. Experiment

1. Samples

Single crystals of α'-NaV_2O_5 were grown from the melt. The detailed procedure is described elsewhere.[26] α'-NaV_2O_5 crystallizes in an orthorhombic unit cell with lattice constants $a=11.318$ Å , $b=3.611$ Å , and $c=4.797$ Å.[2] The vanadium atoms and their five nearest-neighbor oxygen atoms build slightly distorted VO_5 pyramids which are connected by their corners along the **b** direction as well as by their corners and edges along the **a** direction, as shown in Fig. 1(a). The resulting pyramid layers in the ab plane are separated by sodium atoms. The weak interactions between the vanadium oxide layers and the sodium layers are the reason for the good cleavage behavior of this system along the plane perpendicular to the **c** direction. The projection of the vanadium and the oxygen atoms of a single pyramid layer onto the ab plane, excluding the oxygen atoms on the apices of the pyramids, delivers the atomic configuration as illustrated in Fig. 1(b). This approach emphasizes the ladder structure in which adjacent ladders are shifted with respect to each other by half of the lattice parameter b in the **b** direction [see dashed lines in Fig. 1(b)].

For the measurements using electron energy-loss spectroscopy (EELS) in transmission, thin films of about 1000 Å thickness were cut from the single crystals with a diamond knife using an ultramicrotome. Because of the good cleavage behavior, the crystallinity remains conserved after cutting parallel to the ab plane. The high quality and orientation of the single-crystalline samples were checked by *in situ* electron diffraction.

2. EELS in transmission

EELS in transmission with a primary beam energy of 170 keV was performed on free standing films at room temperature (for experimental details, see Ref. 27). The energy and momentum transfer (q) resolution were chosen to be 110

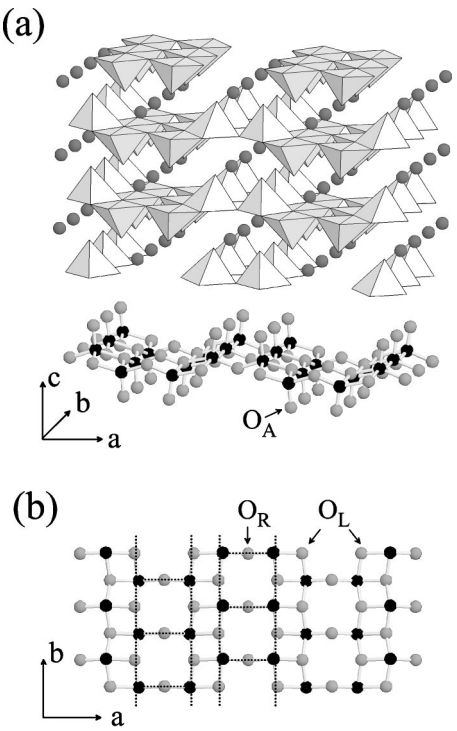

FIG. 1. Crystal structure of α'-NaV_2O_5. Vanadium atoms are shown as black spheres, oxygen atoms as gray spheres. (a) Layers of distorted VO_5 pyramids (upper part) separated by sodium ions (dark gray spheres) and the atomic ordering of a single vanadium oxide layer (lower part). (b) Projection of a single VO-layer onto the ab plane, excluding the apex oxygens. The ladder structure is illustrated by the dashed lines.

meV and 0.05 Å^{-1} for $q \leqslant 0.4$ Å^{-1}, and 160 meV and 0.06 Å^{-1} for $q > 0.4$ Å^{-1}, in order to compensate for the decrease of the cross section at higher momentum transfer.

EELS in transmission provides us with the momentum and energy-dependent loss function $\mathrm{Im}[-1/\varepsilon(\mathbf{q},\omega)]$, from which, by means of the Kramers-Kronig relations, the real part of the negative inverse dielectric function and thus all the optical properties such as, for example, the optical conductivity $\sigma(\omega)$ can be calculated. For small momentum transfer only dipole transitions are allowed, and for the limit $q=0$ the transition matrix elements are the same as in optics. For the Kramers-Kronig analysis the loss spectra closest to the optical limit ($q=0.1$ Å^{-1}) were used in order to derive the optical conductivity spectra.

B. Theory

1. Band-structure calculations

The band structure of α'-NaV_2O_5 was calculated self-consistently using the scalar-relativistic linear muffi-tin orbital (LMTO) method[28] in the atomic sphere approximation with the combined correction taken into account (ASA +CC). The von Barth–Hedin parameterization[29] was used for the exchange-correlation potential constructed in the local spin-density approximation. The Brillouin zone (BZ) integrations in the self-consistency loop were performed using the improved tetrahedron method.[30]

The experimental lattice parameters and atomic positions as determined for the high-temperature phase (Ref. 4) were used in the calculations. The angular momentum expansion of the basis functions included $l=3$ for vanadium and sodium and $l=2$ for oxygen and the empty spheres.[31] The O $3d$ and the V $4f$ states were included in the basis, as they give a significant contribution to the dipole matrix elements of the optical transitions.

In order to account for the strong electronic correlation at the V sites, we used the LSDA+U method in the band-structure calculations,[32] which has been shown to be very helpful for the description of the electronic structure of transition-metal oxides, in which the $3d$ orbitals hybridize quite strongly with the oxygen $2p$ orbitals (for a review, see Ref. 33). In this method a Hubbard-like term is added to the LSDA total-energy functional:

$$E^{\mathrm{LDA}+U}=E^{\mathrm{LSDA}}+E^{U}-E^{\mathrm{dc}}, \tag{1}$$

where E^{LSDA} is the LSDA energy functional, E^U takes into account the on-site Coulomb and exchange interactions, and E^{dc} is necessary to avoid the double counting of the averaged Coulomb and exchange interactions already included in E^{LSDA}.[34] If nonspherical contributions to the on-site Coulomb and exchange integrals U and J are neglected, the E^U term can be written as

$$E^{U}=\frac{1}{2}\sum_{\sigma,i,j\neq i}(U-J)n_{i\sigma}n_{j\sigma}+\frac{1}{2}\sum_{\sigma,i,j}Un_{i\sigma}n_{j-\sigma}, \tag{2}$$

where $n_{i\sigma}$ is the occupancy of the ith localized orbital with the spin projection σ. The localized orbitals used in Eq. (2) are constructed in such a way that they diagonalize the charge density matrix n_{ij}^{σ}. Then, the expression for the orbital-dependent one-electron potential corresponding to Eq. (1) is given by

$$V_{\sigma}^{\mathrm{LDA}+U}=V_{\sigma}^{\mathrm{LSDA}}+\sum_{i}(U-J)\left(\frac{1}{2}-n_{i\sigma}\right)|i\sigma\rangle\langle i\sigma|, \tag{3}$$

where $|i\sigma\rangle\langle i\sigma|$ is the projector onto the localized orbital.

The absorptive part of the optical conductivity tensor components was computed from the LMTO energy bands and eigenvectors on the basis of the linear-response expressions,[35–37] whereas the dispersive part was obtained via the Kramers-Kronig transformation. The finite-lifetime effects and the experimental resolution were simulated by broadening the calculated dielectric tensor spectra with a Lorentzian width of 0.2 eV.

As mentioned in the Introduction, α'-NaV_2O_5 can be considered as composed of linear chains of V-O-V rungs containing a single d electron in a molecular orbital-like state with antiferromagnetic alignment along the ladders. For the LSDA+U calculations presented here, initially an antiferromagnetic (AFM) order of each of the V spins along the leg of the ladder is assumed. We have also carried out a brief analysis of the influence of deviations from this AFM order upon the calculated density of states (DOS) and optical conductivities by means of spin waves. The band-structure calculations for noncollinear magnetic structures including constrained moment directions were performed using the formalism developed in the Refs. 38 and 39. The magnetization direction in the atomic sphere surrounding the site $\mathbf{t}+\mathbf{R}_i$, where $\mathbf{t}$ is its position in the unit cell and $\mathbf{R}_i$ is a real-space lattice vector, is defined by two polar angles θ_{ti} and ϕ_{ti}. If θ_{ti} does not depend on $\mathbf{R}_i$ and ϕ_{ti} is given by

$$\phi_{ti}=\phi_t+\mathbf{u}\cdot\mathbf{R}_i \tag{4}$$

(ϕ_t determines the relative orientation of the magnetization directions for different sublattices), the calculations can be performed without an enlargement of the unit cell for an arbitrary vector $\mathbf{u}$, which defines a spiral magnetic structure in real space. (In the present paper we adopted the notation $\mathbf{u}$ instead of the usually used character $\mathbf{q}$ to distinguish the vector of a spiral structure from the momentum transfer vector in the EELS measurements.) The details of the U calculations for spiral magnetic structures will be given elsewhere.[40] Here we only mention that in this case the effective orbital dependent potential is still given by Eq. (3) but with the spin part of a localized orbital $|i\sigma\rangle$ centered at a given atomic site being defined in the local coordinate system with the z axis parallel to the magnetization direction in the corresponding atomic sphere.

2. Cluster calculations

We have studied the dynamic dielectric response using a quarter-filled t-J-V model

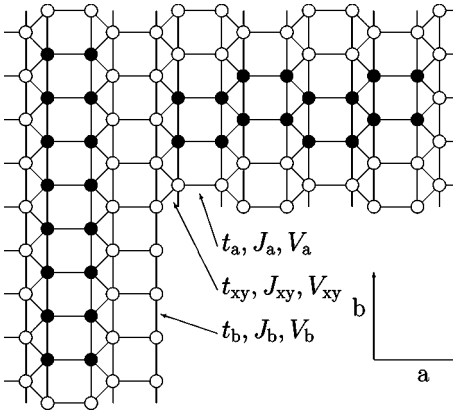

FIG. 2. Schematic structure of the ab planes in α'-NaV_2O_5 where the circles stand for the vanadium sites. The black sites define the two clusters used in the calculation.

$$\mathcal{H} = -\sum_{\langle i,j\rangle,\sigma} t_{ij}(\hat{c}^{\dagger}_{i,\sigma}\hat{c}_{j,\sigma} + \text{H.c.}) + \sum_{\langle i,j\rangle} J_{i,j}\left(\mathbf{S}_i\cdot\mathbf{S}_j - \frac{1}{4}n_i n_j\right) + \sum_{\langle i,j\rangle} V_{i,j} n_i n_j , \tag{5}$$

where $\hat{c}^{\dagger}_{i,\sigma} = c^{\dagger}_{i,\sigma}(1-n_{i,-\sigma})$ are constrained electron creation operators, $n_i = \Sigma_\sigma \hat{c}^{\dagger}_{i,\sigma}\hat{c}_{i,\sigma}$ is the occupation-number operator, and $\mathbf{S}_i$ denotes the spin-$\frac{1}{2}$ operator at site i. The expression $\langle i,j\rangle$ denotes the summation over all pairs of nearest neighbors. The hopping parameters t_{ij}, intersite Coulomb interactions V_{ij}, and exchange interactions J_{ij} are defined in Fig. 2.

The loss function measured in EELS experiments is directly proportional to the dynamic density-density correlation function.[41] By including the long-range Coulomb interaction in the model within a random-phase approximation (RPA) one finds for the loss function

$$L(\omega,\mathbf{q}) = \text{Im}\left[\frac{-1}{1+v_{\mathbf{q}}\chi^0_\rho(\omega,\mathbf{q})}\right], \tag{6}$$

where

$$\chi^0_\rho(\omega,\mathbf{q}) = \frac{i}{\hbar}\int_0^\infty dt\langle 0|[\rho_{\mathbf{q}}(t),\rho_{-\mathbf{q}}]|0\rangle e^{i\omega t} \tag{7}$$

is the response function at zero temperature for the short-range interaction model described by Eq. (5). χ^0_ρ depends on the energy loss ω and momentum transfer $\mathbf{q}$. $|0\rangle$ is the ground state, $\rho_{\mathbf{q}}$ denotes the Fourier transform of n_i, and $v_{\mathbf{q}} = e^2N/(\epsilon_0\epsilon_r v\mathbf{q}^2)$ is the long-range Coulomb potential with unit-cell volume v. Furthermore, N is the number of electrons per unit cell, ϵ_0 is the permittivity, and ϵ_r is the real part of the dielectric function.

We evaluated Eq. (6) by direct diagonalization using the standard Lanczos algorithm.[42] As this method is limited to small clusters, the maximum cluster size in our calculations was restricted to 16 vanadium sites. However, calculations for a cluster consisting of two adjacent ladders, each containing four rungs, showed strong finite-size effects. We have solved this problem by using two different clusters for momentum transfer parallel to **a** and **b** direction, as denoted in Fig. 2 by the filled circles. In the **a** direction we chose an array of double rungs extending over four adjacent ladders, whereas in the **b** direction the cluster consisted of a single ladder with eight rungs. The separation into these two clusters is justified by the small value of the interladder hopping amplitude $t_{xy} = 0.012$ eV (details will be given elsewhere[43]). This value of t_{xy} has also been found by previous LDA calculations,[3] as well as from a tight-binding fit to our own local-density approximation (LDA) results.[44] Additional evidence for a small t_{xy} follows from the weak magnetic dispersion along the **a** direction as observed in neutron-scattering experiments.[6]

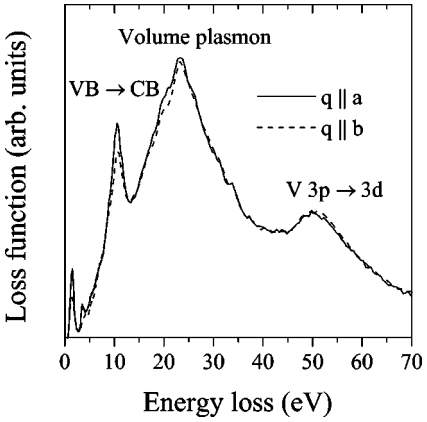

FIG. 3. Electron energy-loss spectra of α'-NaV_2O_5 measured with momentum transfer $\mathbf{q} = 0.1$ Å^{-1} parallel to the crystallographic **a** (solid line) and the crystallographic **b** direction (dashed line).

For the calculation of the loss function we chose open boundary conditions, and for momentum transfer parallel to the **a** direction we used renormalized intersite Coulomb interactions $\overline{V}_a = V_a + V_b$ and $\overline{V}_b = 2V_b$. These values follow from a straightforward analysis of the influence of adjacent rungs of the same ladder on the electronic states.[43] Furthermore, in the case of open boundary conditions one has to make sure that electrons on the edges of the cluster are still embedded in the local Coulomb potential that results from a zigzag charge ordered state. Thus sites on the edge of the cluster for momentum transfer parallel to the **a** direction are assigned an additional on-site energy V_{xy}. By analogy, sites on the edges of the cluster for **q** parallel to the **b** direction need an additional on-site energy V_b, if they are not occupied in a zigzag charge ordered state.

III. RESULTS AND DISCUSSION

A. Loss function with small momentum transfer

We have measured the energy-dependent loss functions for different momentum transfers **q** parallel to the crystallographic **a** and **b** direction in an energy range between 0.5 and 70 eV. Due to the contribution of the elastic line and surface losses it is not possible to measure at zero momentum transfer but close to the optical limit ($q = 0.1$ Å^{-1}). In Fig. 3 the loss functions with momentum transfer $\mathbf{q} = 0.1$ Å^{-1} parallel

to the **a** (solid line) and the **b** direction (dashed line) are shown. Both spectra are dominated by a broad feature at around 23 eV which represents the volume plasmon—a collective excitation of the valence electrons. While the feature at 50 eV results from local excitations between the V $3p$ and the V $3d$ states, the features emerging below the volume plasmon energy can be assigned to transitions of the valence electrons into the conduction band. As Fig. 3 shows, an anisotropic behavior is only visible in the low-energy regime ($\leqslant$22 eV).

In order to compare the spectra with results derived from our LSDA+U calculations, we have calculated the optical conductivity σ by performing a Kramers-Kronig analysis (KKA). The comparison with the optical conductivity of the structurally related V_2O_5 (d^0 configuration) obtained with the same method,[45] shows that above $\sim$5 eV the spectra of both compounds look very similar (not shown). In Ref. 45, the anisotropy of the loss function and of the optical conductivity of V_2O_5 are discussed in detail. As a result, the features above 5 eV can be assigned to transitions from occupied bands with mainly oxygen character into unoccupied bands which are dominated by the V $3d$ states. From the resemblance of the spectra and the related crystal structures of both compounds we conclude that the same holds for α'-NaV_2O_5. Thus in this work we focus on the energy range below 5 eV where the loss functions and, consequently, the optical conductivities of α'-NaV_2O_5 differ strongly from those of V_2O_5.

B. DOS

In comparison to V_2O_5, which has a similar network of linked VO_5 pyramids, the Na atom in α'-NaV_2O_5 donates an additional electron to the valence band. Since in V_2O_5 the bands formed by the O $2p$ states are essentially completely filled and the energetically lowest lying unoccupied bands are formed by the V $3d_{xy}$ states,[45] the additional electron in α'-NaV_2O_5 goes into the rather localized V $3d_{xy}$ states. These states determine, to a great extent, the fascinating properties of this compound. Due to the localized nature of the V $3d$ electrons, the Coulomb correlations between them are rather strong and, as a consequence, conventional L(S)DA calculations fail to describe properly the electronic structure of α'-NaV_2O_5. In the unit cell corresponding to the centrosymmetric $Pmmn$ structure of the high-temperature phase, a nonmagnetic metallic solution is obtained, in contradiction to the experimental data. One way to overcome this discrepancy is to introduce an antiferromagnetic (AFM) order of V magnetic moments along the **b** direction. This leads to a doubling of the unit cell and the opening of an energy gap in the LSDA band structure. However, the value of the energy gap is still strongly underestimated. It should, however, be borne in mind there is no experimental evidence for the existence of AFM order in α'-NaV_2O_5 even at low temperatures.

An efficient way to take the strong correlations in the V $3d$ shell into account is to use the LSDA+U approach. However, this method is usually applied to ordered compounds and thus an additional assumption has to be made in order to study the electronic structure and the optical properties of the high-temperature phase of α'-NaV_2O_5. Since, according to the experimental data, there is no charge ordering above T_c and all V sites are equivalent,[8] we have assumed that the effective one electron potential at each V site is the same and equal to the average of the LSDA+U potentials for V^{4+} and V^{5+} ions. In other words, the orbital-dependent potential is calculated using the occupation numbers averaged formally over the V^{4+} and V^{5+} orbital occupation numbers. On application of U, the partially occupied V d_{xy} orbitals are the most affected. The average occupation of the majority-spin d_{xy} orbitals is close to 0.5 and their energy position remains unchanged as compared to LDA, whereas the unoccupied minority-spin d_{xy} orbitals are shifted upwards by $U/2$. As a result, an insulating behavior—with the magnetic moment of 0.5 μ_B per V atom, or 1 μ_B per rung—is immediately obtained, which is independent of the kind of magnetic order which is assumed along the **b** axis. One can say that the on-site Coulomb repulsion effectively suppresses the occupation of the d_{xy} orbitals with the opposite spin at each rung.

The effect of the absence, in reality, of long-range AFM order in the high-temperature phase of α'-NaV_2O_5 on the electronic structure and optical properties was modelled by performing calculations for spin waves defined by a vector $\mathbf{u}=(0,u_y,0)$ with u_y varying from 0.5 (corresponding to AFM order of V magnetic moments along the **b** direction), to 0 at which all V magnetic moments are ferromagnetically aligned. In these calculations all θ_t were set to zero, whereas the ϕ_t were chosen in such a way that the V ions situated at the same rung had the same magnetization direction. We found that the relative orientation of the magnetization at V sites of neighboring ladders, which is also determined by ϕ_t, has only minor effect on the calculated band structure.

The calculations were iterated to self-consistency for $u_y=0.5$ and then one iteration was performed for spin waves with other values of u_y. The comparison of the band energies confirmed that the ground state of the system is antiferromagnetic, in accordance with previous estimates for the exchange coupling constants between V spins in the **b** direction.

The densities of the V $3d$ and O $2p$ states, calculated for $U_{\mathrm{eff}}=3$ eV and an AFM order of the V magnetic moments along the **b** direction, are shown in Fig. 4. In Fig. 4(b), the density of V $3d$ states calculated for $u_y=0.3$ (dashed lines) is also shown. Here, and in the following, we assume that the magnetic moments of the V ions situated at the same rung are ferromagnetically ordered. The overall structure of the DOS is similar to that of V_2O_5.[45] The states in the energy range from -6.5 to -2 eV are formed mainly by the O $2p$ states [Fig. 4(a)] with a bonding hybridization with the V $3d$ states. The V $d_{xz,yz}$ states dominate in the 1.8–3-eV range, while the states with V $d_{3z^2-r^2}$ and V $d_{x^2-y^2}$ character are shifted to higher energies due to the comparatively strong hybridization with O $2p$ states and form the upper part ($>$3 eV) of the conduction band, shown in Fig. 4(b). The main differences in the structure of the DOS as compared to V_2O_5 are caused by the additional electrons occupying the V

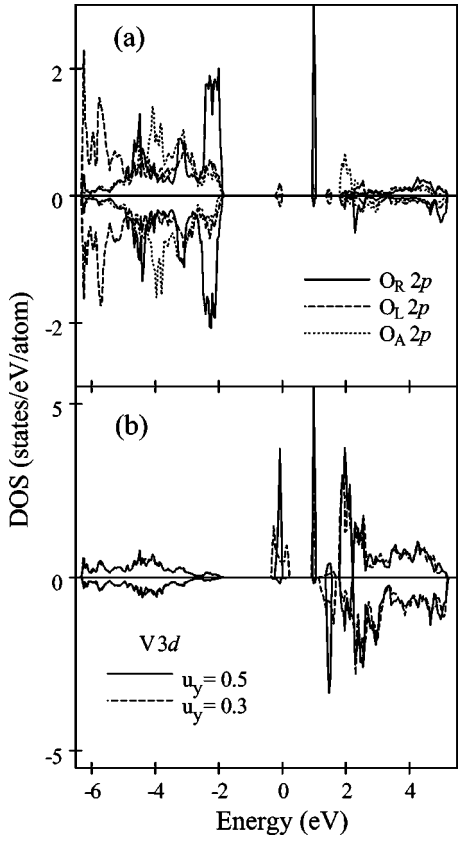

FIG. 4. Spin projected densities of (a) the $2p$ states of the three inequivalent oxygen atoms and (b) the V $3d$ states in α'-NaV_2O_5 calculated for $U_{\text{eff}}=3$ eV and an AFM order of V magnetic moments along the **b** direction. For comparison, the densities of the V $3d$ states calculated with a vector describing the spiral spin structure of $u_y=0.3$ are also shown by dashed lines in (b). All energies are given relative to the valence-band maximum. In the majority-spin V $3d$ DOS the two peaks just below the Fermi level and at 1 eV originate from a bonding and antibonding combination of the $3d_{xy}$ orbitals of the two V atoms on the same rung, respectively. The corresponding combinations of the minority-spin d_{xy} states are shifted to 1.5 and 2.5 eV by the effective Coulomb repulsion.

d_{xy} bands which are empty in the case of V_2O_5. Since the change in the occupation of the V d_{xy} states is the main source of the differences between the optical spectra and other physical properties of these compounds, in the following we will focus our attention on the states originating from the V d_{xy} orbitals.

The narrow peak in the majority-spin V $3d$ DOS just below the Fermi level [Fig. 4(b)] originates from a combination of the $3d_{xy}$ orbitals of the two V atoms on the same rung which is orthogonal to the $2p_y$ orbital of the O_R atom in the center of the rung. The corresponding antibonding V $3d_{xy}$–O_R $2p_y$ states are responsible for the DOS peak at 1 eV. In terms of the effective V–V hopping these two peaks result from the bonding and antibonding combination of the V $3d_{xy}$ states, respectively, and the energy separation between them is determined by $t_a=0.38$ eV acting across the rung. Here, for the effective V–V hopping terms we use the values obtained from a tight binding fit to the LDA band structure

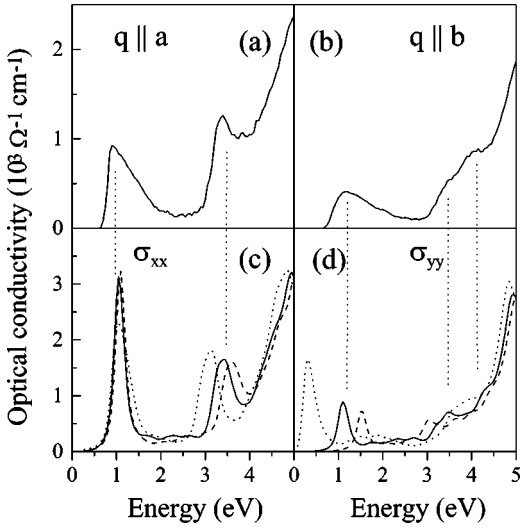

FIG. 5. The optical conductivity of α'-NaV_2O_5. (a) σ_{xx} and (b) σ_{yy} from the EELS experiment. (c) and (d) show the same quantities from the LSDA and LSDA+U band-structure calculations with $U_{\text{eff}}=0$ (dotted line), 2 (solid line), and 3 eV (dashed line). The theoretical curves are broadened with a Lorentzian of width 0.2 eV. The vertical dotted lines illustrate the correspondence of the peak positions.

calculated with the LMTO method,[44] which were found to be very close to the hopping parameters determined in Ref. 3. The minority spin $d_{\downarrow xy}$ states of bonding character are shifted to higher energy by the effective Coulomb repulsion and lie above the antibonding $d_{\uparrow xy}$ peak. While the energy of the latter is governed by t_a and thus does not depend on U_{eff}, the relative position of the minority spin $d_{\downarrow xy}$ states does depend on the exact value of U_{eff}. Finally, the peak at $\sim$2.5 eV arising from the antibonding $d_{\downarrow xy}$ states is almost lost in the contributions from the other states of the conduction band, mainly formed by the remaining V $3d$ states hybridized with O $2p$ states.

It should be noted that for both spin directions the width of the bonding d_{xy} peaks in the LSDA+U calculations is much smaller than 0.7 eV, the value obtained from LDA calculations, because the relatively strong hybridization along the **b** direction governed by $t_b=0.17$ eV is suppressed due to the AFM order. However, as u_y—which defines the magnetic structure along the **b** direction—decreases, the width of the peaks increases and reaches the LDA value when the V magnetic moments are ordered ferromagnetically. As for the antibonding d_{xy} states, the dispersion of the corresponding bands along the Γ–Y direction is much weaker already in LDA,[44] and the width of their DOS does not depend on u_y.

C. Optical conductivity

In order to verify our theoretical results we turn our attention to the optical data. In Fig. 5, the optical conductivity, derived by means of a Kramers-Kronig analysis of the EELS spectra measured at low momentum transfer ($\mathbf{q}=0.1$ Å), aligned either parallel to the crystallographic **a** or **b** direction [Figs. 5(a) and (b)] is shown, together with σ_{xx} and σ_{yy}

calculated for $u_y=0.5$ using the LSDA ($U_{\text{eff}}=0$) and LSDA+U with $U_{\text{eff}}=2$ and 3 eV [Figs. 5(c) and 5(d)]. Our experimental spectra agree well with the previous results derived from reflectivity[17,18] and absorption[16] measurements of α'-NaV_2O_5. Comparing σ_{xx} with the $\mathbf{q}\|\mathbf{a}$ experimental data [Figs. 5(a) and (c)], one can see that for this polarization the theoretical spectra are only weakly affected by U and thus that the LSDA curve agrees well with the experimental one. The calculated position of the low-energy peak in σ_{xx} centered at 1 eV does not depend on U, and coincides almost perfectly with the position of the corresponding experimental maximum. However, the calculations overestimate the magnitude of the peak and fail to reproduce accurately its asymmetric shape. The peak corresponding to the experimental feature at 3.4 eV lies at slightly lower energy in the LSDA calculations and shifts upwards to $\sim$3.7 eV with increasing U.

For σ_{yy} [Figs. 5(b) and 5(d)], the situation is quite different. In this case the LSDA calculations result in an optical gap of 0.2 eV, which is significantly smaller than the experimental value (0.7 eV). In contrast to σ_{xx}, the position of the low-energy peak in σ_{yy} is sensitive to U, and gets close to the experimental value for $U_{\text{eff}}=3$ eV. A less strong but still noticeable dependence on U can be found in the energy range between 2.5 and 4 eV. Comparing the theoretical spectra calculated with different values of U_{eff} to the experimental ones, one can conclude that the best overall agreement between the theory and the experiment is achieved for U_{eff} lying in the range between 2 and 3 eV. This range for U_{eff} derived from the LSDA+U calculations gives an important guideline for the U value taken in the cluster model calculations which will be presented later in the paper.

The observed correspondence between the calculated and the experimental spectra allows us to draw additional information from the detailed analysis of the theoretical spectra. In order to understand better the origins of the features of the optical conductivity and the reasons for their different dependence on the value of U, we analyzed the contributions to the optical conductivity originating from the interband transitions between the initial and final states of V $3d_{xy}$ character. In Fig. 6 we show the results of a decomposition of σ_{xx} and σ_{yy}, calculated with $U_{\text{eff}}=3$ eV. In each case, the thin solid line marks the sum of all the contributions, i.e., the total optical conductivity. Figures 6(a) and 6(c) show the calculations for σ_{xx}, and Figs. 6(b) and 6(d) for σ_{yy}.

Starting with the top two panels [Figs. 6(a) and 6(b)], the areas shaded gray indicate spectral weight connected with transitions starting from the occupied V $3d_{xy}$ bands. Thus it is clear that the lowest lying peaks in both σ_{xx} and σ_{yy} are derived from transitions involving V $3d_{xy}$ *initial* states. The higher lying spectral weight, however, involves transitions starting from O $2p$ states (i.e., the majority of the total σ at higher energy is unshaded).

We turn now to an analysis of the final states involved [see Figs. 6(c) and 6(d)]. In the lower panels of the figure we code the various final state characters with different shading: (i) the antibonding V $3d_{\uparrow xy}$ final states are depicted as light gray; (ii) the bonding V $3d_{\downarrow xy}$ final states are depicted as dark gray, and (iii) the hatched areas show the contributions from interband transitions into higher lying V $3d$ states.

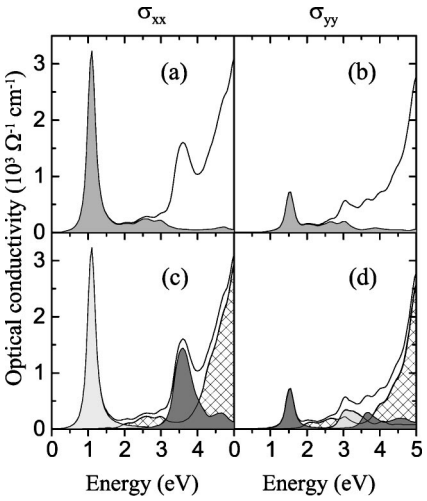

FIG. 6. Decomposition of the optical conductivity of α'-NaV_2O_5 derived from the LSDA+U calculations into contributions arising from transitions involving different initial and final states. In each case panels (a) and (c) show σ_{xx} and (b) and (d), σ_{yy}. The thin solid lines indicate the total optical conductivities. In (a) and (b) the gray shading indicates initial states corresponding to occupied V $3d_{xy}$ bands. In (c) and (d) light gray (dark gray) shading indicates antibonding V $3d_{\uparrow xy}$ (bonding V $3d_{\downarrow xy}$) final states. The hatched area shows the contribution from interband transitions into higher lying empty V $3d$ states.

On comparing the top and bottom panels of Fig. 6 we can therefore conclude the following about the transitions giving rise to the optical conductivity. First, the 1-eV peak in σ_{xx} is due to a transition between bonding and antibonding hybrids involving the V d_{xy} levels of equal spin direction. As was mentioned above, the bonding-antibonding splitting of d_{xy} states is determined only by the hybridization within a rung and is thus *not* affected by U.

Second, for momentum transfer parallel to the **b** direction, the matrix elements for the bonding-antibonding transitions are zero. In this case, transitions between bonding V d_{xy} levels with opposite spin become active. The energy position of these transitions is sensitive to the strength of the on-site Coulomb interaction, which naturally explains the strong dependence of the position of the low energy peak in σ_{yy} on the value of U observed in Fig. 5. In the language of a many-body approach, the $d_{\uparrow xy}\rightarrow d_{\downarrow xy}$ transitions can be thought of as excitations which lead to the creation of doubly occupied rungs.[46]

Having dealt with the low-lying features of the optical conductivity, we now turn our attention to the energy range between 3 and 4 eV. In this context, the lack of gray shaded weight in Figs. 6(a) and 6(b) illustrates that the initial states of the transitions responsible for σ in this energy range have O $2p$ character. Consideration of Figs. 6(c) and 6(d) reveals that the peak in σ_{xx} at 3.7 eV and the small hump in σ_{yy} at the same energy are dominated by transitions into the $d_{\downarrow xy}$ bands (dark gray shaded spectral weight). The initial and final states of the transitions giving rise to σ_{xx} between 3 and 4 eV are, in fact, of the same character as those which de-

TABLE II. Energy positions and character of the electronic transitions contributing to the optical conductivities σ_{xx} and σ_{yy} of α'-NaV_2O_5 in the low-energy range.

E (eV)	σ_{xx}	σ_{yy}
1.1	V $3d_{\uparrow xy} \rightarrow$ V $3d_{\uparrow xy}$	
1.5		V $3d_{\uparrow xy} \rightarrow$ V $3d_{\downarrow xy}$
3.1		O $2p \rightarrow$ V $3d_{\uparrow xy}$
3.7	O $2p \rightarrow$ V $3d_{\downarrow xy}$	O $2p \rightarrow$ V $3d_{\downarrow xy}$
2–3	V $3d_{\uparrow xy} \rightarrow$ V $3d_{xz,yz}$	V $3d_{\uparrow xy} \rightarrow$ V $3d_{xz,yz}$

termine the shape of the σ_{xx} spectrum in V_2O_5 just above the absorption threshold.[45] The dipole transitions from the O $2p$ valence-band states into the antibonding $d_{\uparrow xy}$ states are completely suppressed for a polarization parallel to **a** (σ_{xx}), while for σ_{yy} they play an important role in the formation of the shoulder in this energy range [shaded light gray in Fig. 6(d)].

Finally, we mention that transitions from the occupied d_{xy} bands to that part of the conduction band originating from the V $d_{xz,yz}$ states give rise to the nonvanishing intensity in the calculated spectra in the energy range between the main features (i.e., between 1.5 and 3 eV). The experimental σ's [see Figs. 5(a) and 5(b)] confirm the accuracy of the theoretically predicted optical conductivity in this regard.

In order to summarize the detailed information won in this section as regards the character of the states involved in the transitions giving rise to both σ_{xx} and σ_{yy} in a concise form, Table II shows a breakdown including the respective initial and final states ''behind'' each spectral feature.

The level to which the detailed breakdown of the calculated optical conductivity has been carried out in Fig. 6 is justified by the fact that the theoretical curves (for example the solid line) in Fig. 5 are able not only to reproduce the main features in σ_{xx} and σ_{yy} quite well, but also the weaker, double peak structure in σ_{yy} in the 3–4 eV range in our experimental data [see Fig. 5(b)]. We note that the spectra derived from optical measurements did not resolve this double-peak feature.[17]

Despite the quite good agreement between the calculated and measured optical conductivity on the qualitative level, the absolute magnitude and strongly asymmetric shape of the low-energy peaks in σ_{xx} and σ_{yy} are not accurately reproduced by the calculations (see Fig. 5). We point out two possible sources for these discrepancies: (i) an oversimplified treatment of the charge fluctuations in the high-temperature phase using an averaged one-electron potential and (ii) the assumption that the V magnetic moments are antiferromagnetically aligned along the **b** direction. Dealing first with the issue of the charge fluctuations, we note that a more rigorous treatment of the charge disorder on the V sublattice of α'-NaV_2O_5 is beyond the capabilities of the LSDA+U approach in its present formulation. We therefore return to this question later in the paper in the context of the cluster calculations which will be described in detail in the next but one subsection. As regards the influence of deviations from long-range AFM order on the optical spectra, we point out that the

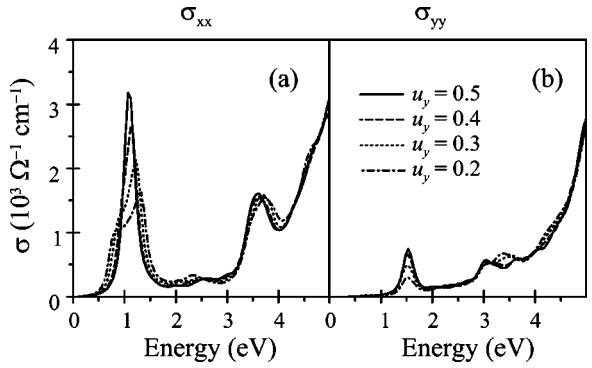

FIG. 7. Optical conductivity of α'-NaV_2O_5 calculated for $U_{\text{eff}}=3$ eV and different values of u_y, which defines the magnetic structure along the **b** direction (for details see text).

strength of such effects can be estimated by performing calculations for a spin-wave structure along the b axis.

The optical conductivity spectra calculated for $U_{\text{eff}}=3$ eV and for different values of the vector describing the spiral magnetic structure in real space u_y are shown in Fig. 7. Since the change of the magnetic structure affects the bands formed from the V d_{xy} bonding states most strongly (see Fig. 4), the spectral features originating from the transitions in which these bands are involved demonstrate the strongest dependence on u_y. In particular, the change in shape and intensity of the peak at 1 eV in σ_{xx} [Fig. 7(a)] is the most noticeable result of including spiral spin structures along the b axis. As can be seen from the figure, as u_y decreases, the peak becomes less intensive and its maximum shifts to higher energy. Since the final states for the corresponding transitions (i.e., the antibonding V d_{xy} states) remain very narrow independent of the nature of the magnetic order along the **b** direction, the increase in the width of the peak reflects the change of the density of the occupied V d_{xy} states (i.e., the initial states). The shape of the low energy peak in σ_{yy} [Fig. 7(b)] does not change with increasing u_y but its intensity rapidly decreases as u_y decreases, and vanishes completely for $u_y=0$ at which point the V magnetic moments order ferromagnetically. The drop of intensity of the low-lying feature in σ_{yy} is caused by the decrease of the weight of majority-spin states in the final-state wave functions. For $u_y=0$ the initial and final states are formed by pure majority- and minority-spin states, respectively, and the corresponding transitions are forbidden (since the relativistic effects were not included in the calculations). The spectral features in the energy range between 3 and 4 eV are also influenced by u_y, but the changes are less pronounced than for the low-lying features.

The comparison of the calculated optical conductivity with inclusion of the spin spiral structures (Fig. 7) with the experimental spectra [Figs. 5(a) and 5(b)] indicates that an improved agreement between the theoretical and experimental magnitude of the low-energy peaks of σ_{xx} and σ_{yy} can be achieved if deviations from pure AFM order along the **b** axis are taken into account. However, even including spin-waves, the LSDA+U results are unable to fully account for the asymmetric shape of the low-energy peaks in the experimental optical conductivities.

To try to overcome this weakness, we have also calculated the optical conductivity for different relative orientations of the magnetization at neighboring ladders (not shown). The changes of the calculated spectra were found to be very small, which is in keeping with the size of the interladder hopping term ($t_{xy}=0.012$ eV) which couples V ions belonging to neighboring ladders.

To bring this section on the data from band-structure calculations to a close, the LSDA+U results regarding the optical properties of α'-NaV_2O_5 can be summarized as follows.

(i) The optical conductivities σ_{xx} and σ_{yy} calculated with U_{eff} in the range between 2 and 3 eV are able to reproduce the main features of the experimental spectra, as well as the observed optical anisotropy quite well. This fact indicates the relevance and accuracy of the parameters determined both from the fit to the band structure (the transfer integrals, or t's) or from the comparison with the experiment (U).

(ii) The analysis of the contributions to σ coming from interband transitions with different initial and final states allows us to determine the electronic states responsible for the formation of the peaks in the experimental optical conductivity. Table II summarizes this information for each spectral feature in σ_{xx} and σ_{yy}.

(iii) However, the remaining discrepancy between the theory and the experiment as regards the shape of the low-energy peaks (even despite going beyond the AFM approximation for the spin order along **b**) indicates that the subtle details of the electronic structure of the high-temperature phase of α'-NaV_2O_5 are beyond the approximations inherent to the LDA, and thus are most likely sensitive to effects more suitably treated within the framework of models in which electronic correlation is dealt with at a more fundamental level.

Before going on to the *t*-*J*-*V* model cluster calculations presented in the last sub-section of the results and discussion part of the paper, the next subsection deals with the first EELS spectra of α'-NaV_2O_5 recorded beyond the optical limit. Here we exploit the strength of EELS in transmission as a measure of the bulk optical properties (in this case of α'-NaV_2O_5) for finite momenta, thus giving additional insight into the nature of the two-particle excitations in this complex system.

D. Momentum-dependent loss functions

In the left panels of Fig. 8, we show the EELS loss function of α'-NaV_2O_5 recorded for different values of **q**, either parallel to the crystallographic **a** [Fig. 8(a)] or **b** [Fig. 8(c)] direction. The spectra are normalized at higher energy (ca. 7 eV) where the shape of the spectra does not change either with the absolute value or with the direction of the momentum transfer (see also Fig. 3). For clarity the spectra are incrementally offset in the y direction.

For **q** parallel to both the **a** and **b** directions the spectra show strong intensity between the spectral onset at 0.7 eV up to 2 eV, as well as additional weaker features located between 3 and 4.5 eV. For small **q** the corresponding plasmon excitations are related to the same dipole transitions which

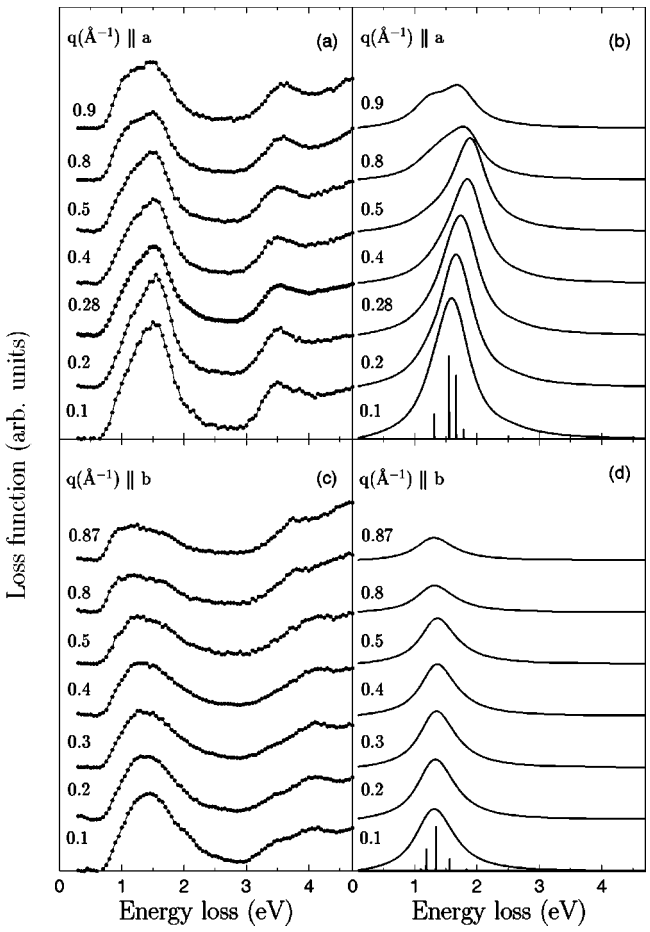

FIG. 8. Panels (a) and (c) show the loss function of α'-NaV_2O_5 measured using EELS with momentum transfer aligned along the **a** and **b** directions, respectively. Panels (b) and (c) show the corresponding calculated loss functions from a quarter filled *t*-*J*-*V* model, which have been broadened with a Gaussian function of width 0.3 eV. For the $q=0.1$ Å^{-1} calculated spectra, an unbroadened version has also been plotted to enable indentification of the individual plasmons. For the parameters used in the calculation, see text.

are responsible for the peaks at around 1 and 3.5 eV in the optical conductivities whose origin was discussed in detail above. In the following, we concentrate our attention on the fine structure of the low-energy peaks, as well as on the dependence of the shape and position of the peaks on the increasing momentum transfer.

First, we focus on the features below 2 eV. The intensities in the **a** direction are about two times larger than those with the same momentum transfer in the **b** direction. For **q**$\|$**a**, the maximum lies at 1.55 eV compared with 1.45 eV for **q**$\|$**b**. At high momentum transfers the fine structure of the feature around 1.5 eV in the **a** direction indicates the presence of transitions into more than a single final state. One can distinguish between essentially three features, whereby the intensity of the component with its maximum at 1.55 eV decreases more rapidly with q than the features at 1.2 and 1.7 eV, the latter pair being visible as weak shoulders only for high-momentum transfers. In the **b** direction the low energy feature is also composed of more than one component—at

least at high **q**. The energetically lowest lying feature (at $\sim$0.9 eV)—which can be seen as a shoulder at $q \geqslant 0.4$ Å^{-1}—loses intensity only slowly with increasing q. The second component, which one can relate to the main intensity maximum (ca. 1.3 eV) decreases more strongly in intensity at higher q. Last, for $q \geqslant 0.5$ Å^{-1}, a third component is visible at higher energy (ca. 1.7 eV).

Finally, we turn to the features in the loss function at energies above 3 eV, which, as in the data recorded at the low-q limit, are clearly separated from the lower energy features by a strong drop of spectral weight between 2 and 3 eV. In the **a** direction a steep increase of spectral weight occurs at 3 eV, which evolves into a maximum at 3.5 eV. With increasing momentum transfer the peak position of this feature does not change and the intensity decreases slowly. A peak at the same energy position with a similar shape was observed for the **a** as well as for the **b** direction in the loss functions of V_2O_5, and is assigned to transitions from the O $2p$ states into the lowest unoccupied V $3d_{xy}$ states.[45] However, in the EELS spectra of α'-NaV_2O_5, the shape of the corresponding feature in the **b** direction differs by the presence of a double-peaked structure with maxima at 3.5 and 5.1 eV. The two peaks merge together with increasing momentum transfer, and for $q \geqslant 0.7$ Å^{-1} a further feature becomes visible at $\sim$3.8 eV. Since in electron energy-loss spectroscopy the cross section for dipole transitions decreases and that for dipole forbidden transitions increases with increasing momentum transfer, the latter 3.8-eV feature is most likely related to monopole or quadrupole transitions.

Having described the experimental loss functions as a function of momentum, we now discuss the results of the cluster model calculations aimed at their simulation.

E. Calculated loss functions

In Fig. 8 the results of our cluster calculations (see Sec. II B 2) are compared with the experimental spectra.[47] Such cluster calculations require, naturally, input parameters which in turn describe the essentials of the physics of the system in question. In this case, for the transfer integrals we take the values $t_a = 0.38$ eV, $t_b = 0.17$ eV, $t_{xy} = 0.012$ eV from our tight-binding fit to the band-structure calculations mentioned earlier. These values are identical to those of Ref. 3. A further, vital parameter is the on-site Coulomb repulsion, U. Here we take a value of 2.8 eV—a choice which is guided by the range of $U_{\mathrm{eff}} = 2-3$ eV which came out of the LSDA+U calculations presented and discussed above.

At this stage we can have faith in these parameters for two reasons. First, it is well known that LDA does a good job in describing the charge distribution, and hence the hybridization/transfer integrals, even in systems with strong electronic correlation. Second, the good basic agreement between the optical conductivity calculated within LSDA+U with experiment (see Sec. III C) not only lends support to the t's, but underpins the chosen U value.

The exchange interactions were parametrized as $J_{ij} = 4t_{ij}^2/U$ and the values of the intersite Coulomb interactions $V_a = 0.8$ eV and $V_b = 0.6$ eV fulfill the condition for the system to be close to a quantum critical point caused by charge ordering, as described by Cuoco *et al.*[22] The interladder Coulomb interaction $V_{xy} = 0.9$ eV has been adjusted within the model to obtain the correct peak positions with respect to the experimental loss functions. To allow a direct comparison with experiment, the calculated data were broadened with a Gaussian function of 0.3-eV width. The unbroadened spectra for $\mathbf{q} = 0.1$ Å are also shown as vertical lines in Figs. 8(b) and 8(d). As the cluster model contains only V sites, we only attempt to simulate the loss function in the low-energy range (i.e., for <3 eV). At higher energies—as we know from our combined analysis of the experimental and theoretical optical conductivities (Sec. III C)—excitations from O $2p$ to V $3d$ orbitals play a role. Thus this spectral weight cannot be described within the present cluster model.

We find a good agreement between theory and experiment for the low-energy part of the loss function for $\mathbf{q} \| \mathbf{a}$, in particular for the data recorded at higher q [see Figs. 8(a) and 8(b)]. Specifically, the intensity reduction and increasing width of the experimentally observed structure between 1 and 2 eV for $q > 0.5$ Å^{-1} is well reproduced in the cluster calculation, a characteristic which eluded our best efforts within the LSDA+U approach. For the calculated loss function with $\mathbf{q} \| \mathbf{b}$ [Fig. 8(d)], the experimental q-dependent reduction in intensity is also well reproduced. However, in this case the simulation fails to reproduce accurately the large width of the low-energy feature—a shortcoming which becomes increasingly apparent for higher q.

In order to enable a discussion of the origin of the individual features underlying the calculated spectra, one should note that since α'-NaV_2O_5 is close to a charge order transition,[22] one can describe the nature of the excitations using a zigzag ordered ground state. In this context, we mention that excitations with momentum transfer parallel to the **a** direction lead to a disturbance of the charge ordering as they involve hopping of electrons from one side of a rung to the other. Note that this process can also be interpreted as a transition from a bonding to an antibonding state of a singly occupied rung, in agreement with the results from recent calculations using the Heitler-London model.[48] Since the net interladder Coulomb interaction V_{xy} remains unchanged after the hopping on the rung in the charge ordered state, the excitation energy is dominated by V_b. In addition to the one electron hopping discussed above, there are also collective processes that involve two or three neighboring rungs on different ladders.

As the unbroadened theoretical results presented in Fig. 8(b) show, the theoretical spectra consist of three main features, each of which can be attributed to a density oscillation (plasmon) with energies between 1 and 2 eV. For $\mathbf{q} \| \mathbf{a}$, the spectral weight shifts from the plasmon at 1.6 eV to the one at 1.7 eV with increasing **q**, which makes it appear as if the low-lying feature as a whole disperses to higher energy, which is not, in fact, the case. The three excitations differ in their degree of delocalization. The excitation at 1.3 eV is related to rather delocalized transitions involving more than one electron in the cluster. The higher lying plasmons, however, result from more localized processes.

For momentum transfer parallel to the **b** direction, the excitations contributing to the low lying spectral weight [see Fig. 8(d)] can be interpreted as transitions from a state in which two rungs are singly occupied to one in which one rung is empty and the other doubly occupied. Due to the finite hopping amplitude $t_b = 0.17$ eV, the unoccupied and the occupied rung are able to move along the ladder independently from each other. Thus many more final states are available in the **b** direction than in the **a** direction. The energies of the transitions into these final states depend on the distance between the unoccupied and the doubly occupied rung. However, since we can observe only localized excitations by the direct diagonalization of small clusters, we are unable to capture fully the dynamics of these excitations and thus we miss some spectral weight (in the form of spectral breadth) in the theoretical spectra [Fig. 8(d)] compared to the experimental data [Fig. 8(c)]. This explanation is supported by a further reduction of spectral weight in the cluster calculation when we adopt a four-rung ladder, in place of the eight rung cluster from which the results are presented here.

Thus, in contrast to the good description of the strongly localized excitations in the **a** direction described earlier, for $\mathbf{q} \| \mathbf{b}$ we find that the theory significantly underestimates the spectral weight, due to finite-size effects in the cluster calculation. That these differences also persist in the high q regime illustrates that the cluster size imposes limitations even in the case where the excitations have shorter wavelength. Nevertheless, it should be pointed out that the cluster calculations do provide a qualitative description of both position and the q-dependent decrease of intensity of the experimental features.

The optical conductivity can also be calculated using the same, cluster-based method. With the same model parameters we obtain a qualitative agreement with the optical conductivity, either as derived from EELS or optical measurements[17] (not shown). However—as was the case for the LSDA+U data—the asymmetric line shape in σ could not be fully reproduced in the cluster calculation. We ascribe this to the delocalized character of some of the final states, which at $\mathbf{q} = 0$ (i.e., at infinite wavelength) therefore elude our calculations based upon a finite cluster. We note here that a similar type of calculation has been carried out recently,[22] and a good agreement between theory and the $(q = 0)$ optical conductivity was found, albeit with a rather high value of the interladder hopping integral $t_{xy} = 0.15$ eV. The momentum-dependent EELS data presented here allow a further test of the theoretical parameters beyond the optical limit. We have found that adopting $t_{xy} = 0.15$ eV in our *t*-*J*-*V* model calculations yields a significantly worse agreement with the experimental data than does the value of $t_{xy} = 0.012$ eV, which also comes out of the tight-binding fit to the band structure. Consequently, it appears as if a large value of the interladder hopping is not a requirement for an accurate description of the charge excitations in α'-NaV_2O_5.

To summarize, one can say that while the small interladder hopping gives a rationale for the quasi-one-dimensional character of the dynamics of the V $3d$ electrons; the fact that all three intersite Coulomb interactions (V_a, V_b, and V_{xy}) are of similar size is consistent with the two-dimensional nature of the charge ordering occurring at low temperatures in this system.

IV. SUMMARY

In conclusion, we have presented a joint experimental and theoretical investigation of the optical properties and collective excitations of α'-NaV_2O_5. From measurements by means of high-resolution EELS in transmission, we have derived σ_{xx} and σ_{yy} in the optical limit and have also presented the momentum dependence of the loss function with momentum transfers parallel to the crystallographic **a** and **b** directions. The densities of states and optical conductivities were calculated within an LSDA+U framework, with the spin order at the V sites either described in terms of an antiferromagnetic or spin-wave-like arrangement, whereas the momentum-dependent loss functions were simulated using a quarter-filled *t*-*J*-*V* model based upon a cluster of 16 vanadium sites.

For **q** parallel to both the **a** and **b** directions, the low energy features of the spectra are essentially dispersionless—which is in keeping with the small bandwidth of the unoccupied states directly above the chemical potential predicted in the LSDA+U calculations. The comparison between the experimental σ's (measured in the optical limit) and those derived from the LSDA+U calculations yielded a good agreement upon adoption of an on-site Coulomb interaction $U = 2-3$ eV and an antiferromagnetic ordering of the spins at the V sites in the ladders. However, the LDA-based calculations were not able to reproduce the width of the experimentally observed structures.

Based upon the LSDA+U results, the differences between σ_{xx} and σ_{yy} could be analyzed in detail and each feature could be characterized according to the nature of the initial and final states involved in the underlying optical transitions. For example, it could be shown that the optical conductivity between 0.5 and 1.7 eV is dominated by transitions from the highest occupied band (bonding combination of V $3d_{xy}$ states) into the lowest unoccupied band (antibonding V $3d_{xy}$-O_R $2p_y$ states). While for σ_{xx} such an excitation occurs on a single rung, in σ_{yy} the same transition can be considered as a hopping process to one of the adjacent rungs. The higher lying features in the optical conductivity (above 3 eV) are shown to be related to transitions originating in the O $2p$ valence band manifold.

Taking the transfer integrals and U value from our LSDA+U data (the accuracy of which is checked by the comparison with the experimental σ's), the *t*-*J*-*V* cluster model was successful in describing the q dependence of the intensity and, in particular the observed width of the lowest energy feature at high q for $\mathbf{q} \| \mathbf{a}$. As the high q data probe shorter wavelengths, it is clear that the cluster extension in the **a** direction is sufficient to describe these localized excitations. The situation is different for the data with $\mathbf{q} \| \mathbf{b}$. Here the cluster calculation manages to reproduce the q dependence of the intensity well, but still fails to correctly account for the width of the experimentally observed feature at high

q, thus signalling the impact of finite-size effects, even in a 16 site cluster.

The analysis of the momentum dependence of the loss function allows a more precise determination of the values of the model parameters. The best agreement is achieved with transfer integrals which mirror those derived from the band-stucture calculation. In particular, the interladder hopping, t_{xy} is found to be 0.012 eV, thus confirming the quasi one-dimensional nature of the electronic system in α'-NaV_2O_5. Finally, the intersite Coulomb interactions V_a, V_b, and V_{xy} are found to be of similar magnitude. These interactions then drive the electronic system close to a quantum critical point between a unordered state at room temperature and a zigzag ordered state[49] observed at low temperatures.

ACKNOWLEDGMENT

We are grateful to the Deutsche Forschungsgemeinschaft for financial support under contract numbers DFG Fi-439/7-1 and DFG Ho-955/2-3.

*Permanent address: Institute of Metal Physics, 36 Vernadskii str., 252142 Kiev, Ukraine.

[1] M. Isobe and Y. Udea, J. Phys. Soc. Jpn. **65**, 1178 (1996).
[2] P. A. Carpy, A. Casalot, M. Pouchard, J. Galy, and P. Hagenmuller, J. Solid State Chem. **5**, 229 (1972); P. A. Carpy, and J. Galy, Acta Crystallogr., Sect. B: Struct. Crystallogr. Cryst. Chem. **31**, 1481 (1975).
[3] H. Smolinski, C. Gros, W. Weber, U. Peuchert, G. Roth, M. Weiden, and C. Geibel, Phys. Rev. Lett. **80**, 5164 (1998).
[4] H. G. von Schnering, Yu. Grin, M. Kaupp, M. Somer, R. K. Kremer, O. Jepsen, T. Chatterji, and M. Weiden, Z. Kristallogr. **213**, 246 (1998).
[5] Y. Fujii, H. Nakao, T. Yosihama, M. Nishi, K. Nakajima, K. Kakurai, M. Isobe, Y. Ueda, and H. Sawa, J. Phys. Soc. Jpn. **66**, 326 (1997).
[6] T. Yosihama, M. Nishi, K. Nakajima, K. Kakurai, Y. Fuji, M. Isobe, C. Kagami, and Y. Ueda, J. Phys. Soc. Jpn. **67**, 744 (1998).
[7] K. Kobayashi, T. Mizokawa, A. Fujimori, M. Isobe, and Y. Ueda, Phys. Rev. Lett. **80**, 3121 (1998).
[8] T. Ohama, H. Yasuoka, M. Isobe, and Y. Ueda, J. Phys. Soc. Jpn. **66**, 3008 (1997).
[9] H. Seo and H. Fukuyama, J. Phys. Soc. Jpn. **67**, 2602 (1998).
[10] M. V. Mostovoy and D. I. Khomskii, Solid State Commun. **113**, 159 (2000).
[11] M. J. Konstantinović, Z. V. Popović, A. N. Vasil'ev, M. Isobe, and Y. Ueda, Solid State Commun. **112**, 397 (1999).
[12] H. Nakao, K. Ohwada, N. Takesue, Y. Fujii, M. Isobe, Y. Ueda, M. v. Zimmermann, J. P. Hill, D. Gibbs, J. C. Woicik, I. Koyama, and Y. Murakami, Phys. Rev. Lett. **85**, 4349 (2000).
[13] T. Ohama, A. Goto, T. Shimizu, E. Ninomiya, H. Sawa, M. Isobe, and Y. Ueda, J. Phys. Soc. Jpn. **69**, 2751 (2000).
[14] H. Lohmann, H.-A. Krug von Nidda, M. V. Eremin, A. Loidl, G. Obermeier, and S. Horn, Phys. Rev. Lett. **85**, 1742 (2000).
[15] J. Lüdecke, A. Jobst, S. van Smaalen, E. Moré, C. Geibel, and H.-G. Krane, Phys. Rev. Lett. **82**, 3633 (1999).
[16] S. A. Golubchik, M. Isobe, A. N. Ivlev, B. N. Mavrin, M. N. Popova, A. B. Sushkov, Y. Ueda, and A. N. Vasil'ev, J. Phys. Soc. Jpn. **66**, 4042 (1997); **68**, 318 (1999).
[17] A. Damascelli, D. van der Marel, M. Grüninger, C. Presura, T. T. M. Palstra, J. Jegoudez, and A. Revcolevschi, Phys. Rev. Lett. **81**, 918 (1998).
[18] V. C. Long, Z. Zhu, J. L. Musfeldt, X. Wei, H.-J. Koo, M.-H. Whangbo, J. Jegoudez, and A. Revcolevschi, Phys. Rev. B **60**, 15 721 (1999).
[19] Z. S. Popović and F. R. Vukajlović, Phys. Rev. B **59**, 5333 (1999).
[20] H. Wu and Q. Zhang, Phys. Rev. B **59**, 15 027 (1999).
[21] N. Katoh, T. Miyazaki, and T. Ohno, Phys. Rev. B **59**, R12 723 (1999).
[22] M. Cuoco, P. Horsch, and F. Mack, Phys. Rev. B **60**, R8438 (1999).
[23] S. Nishimoto and Y. Ohta, J. Phys. Soc. Jpn. **67**, 3679 (1998).
[24] S. Nishimoto and Y. Ohta, J. Phys. Soc. Jpn. **67**, 4010 (1998).
[25] P. Horsch and F. Mack, Eur. Phys. J. B **5**, 367 (1998).
[26] M. Lohmann, A. Loidl, M. Klemm, G. Obermeier, and S. Horn, Solid State Commun. **104**, 649 (1997).
[27] J. Fink, Adv. Electron. Electron Phys. **75**, 121 (1989).
[28] O. K. Andersen, Phys. Rev. B **12**, 3060 (1975).
[29] U. von Barth and L. A. Hedin, J. Phys. C **5**, 1629 (1972).
[30] P. E. Blöchl, O. Jepsen, and O. K. Andersen, Phys. Rev. B **49**, 16 223 (1994).
[31] To diminish the overlap between atomic spheres 12 additional empty spheres were inserted into the simple orthorhombic unit cell of α'-NaV_2O_5.
[32] V. I. Anisimov, I. V. Solovyev, M. A. Korotin, M. T. Czyzyk, and G. A. Sawatzky, Phys. Rev. B **48**, 16 929 (1993).
[33] V. I. Anisimov, F. Aryasetiawan, and A. I. Lichtenstein, J. Phys.: Condens. Matter **9**, 767 (1997).
[34] A. I. Lichtenstein, V. I. Anisimov, and J. Zaanen, Phys. Rep. **52**, R5467 (1995).
[35] R. Kubo, J. Phys. Soc. Jpn. **12**, 570 (1957).
[36] E. G. Maksimov, I. I. Mazin, S. N. Rashkeev, and Y. A. Uspenskii, J. Phys. F **18**, 833 (1988).
[37] V. N. Antonov, A. I. Bagljuk, A. Ya. Perlov, V. V. Nemoshkalenko, Vl. N. Antonov, O. K. Andersen, and O. Jepsen, J. Low Temp. Phys. **19**, 494 (1993).
[38] L. M. Sandratskii, Phys. Status Solidi B **136**, 167 (1986).
[39] S. V. Halilov, H. Eschrig, A. Y. Perlov, and P. M. Oppeneer, Phys. Rev. B **58**, 293 (1998).
[40] A. Yaresko, A. Y. Perlov, R. Hayn, and H. Rosner (unpublished).
[41] S. E. Schnatterly, Solid State Phys. **34**, 275 (1977).
[42] See, for example, H. Q. Lin and J. E. Gubernatis, Comput. Phys. **7**, 400 (1993), and references therein.
[43] A. Hübsch, C. Waidacher, K. W. Becker, and W. von der Linden (unpublished).
[44] A. N. Yaresko, V. N. Antonov, H. Eschrig, P. Thalmeier, and P. Fulde, Phys. Rev. B **62**, 15 538 (2000).
[45] S. Atzkern, M. Knupfer, M. S. Golden, J. Fink, A. N. Yaresko, V. N. Antonov, M. Klemm, and S. Horn, Phys. Rev. B **61**, 12 792 (2000).

[46] In order to avoid misunderstanding, we note here that due to the AFM order imposed along the **b** direction, the states with both spin projections contribute to the Bloch wave functions and thus the bands are labeled as majority and minority spin only for convenience according to the dominating contribution of the d_{xy} states at a chosen V site. In view of this remark the term ''$d_{\uparrow xy} \rightarrow d_{\downarrow xy}$ transition'' does not imply that the transition occurs between the states with opposite spins, which would become possible if the relativistic effects were taken into account, but simply specifies the initial and final bands involved in the transition.

[47] The broadened theoretical curves for $q = 0.1$ Å^{-1} in Figs. 8(b) and 8(d) have been scaled to match the intensity of the experimental data. The intensity development of the cluster results as a function of **q**, however, is left unadjusted and is therefore a valid result of the calculations.

[48] C. Presura, D. van der Marel, A. Damascelli, and R. K. Kremer, Phys. Rev. B **62**, 16 522 (2000).

[49] M. Vojta, R. E. Hetzel, and R. M. Noack, Phys. Rev. B **60**, R8417 (1999).

[50] D. Sa and C. Gros, Eur. Phys. J. B **18**, 421 (2000).